Effect of Constrained Annealing on the Mechanical Properties of Electrospun Poly(ethylene oxide) Webs Containing Multiwalled Carbon Nanotubes

Jiaxing Bao,[1] Laura I. Clarke,[2] Russell E. Gorga[1,3]

[1]Textile Engineering, Chemistry and Science, NC State University, Raleigh, North Carolina, 27695
[2]Department of Physics, NC State University, Raleigh, North Carolina, 27695
[3]Fiber and Polymer Science Program, NC State University, Raleigh, North Carolina, 27695
Correspondence to: R. E. Gorga (E-mail: regorga@ncsu.edu) or L. I. Clarke (E-mail: liclarke@ncsu.edu)

Received 21 July 2015; accepted 17 October 2015; published online 24 November 2015
DOI: 10.1002/polb.23960

ABSTRACT: In this work, flexible nanofibrous membranes (mats) of poly(ethylene oxide) (PEO) with and without multiwall carbon nanotubes (MWNTs) were fabricated by electrospinning. The effects of annealing and MWNT concentration on mat morphology, MWNT dispersion within the nanofibers, and the mechanical properties of electrospun mats were studied. Annealing temperatures ranged from 60 °C to 64 °C [near the melting temperature (64 °C via differential scanning calorimetry)] for 4 minutes. Samples were annealed with and without applied tension (constrained and unconstrained annealing). Annealing at the highest temperature (64 °C), before the loss of fibrous morphology, significantly improved fiber–fiber bonding and therefore the tensile strength of the mats. Compared with unconstrained annealing, constrained annealing introduced fiber alignment (and therefore molecular orientation) along the tensile axis (direction of constraint) during annealing and resulted in a significant increase in modulus for all samples (with and without MWNTs). The use of constrained annealing may be a facile approach to enhance modulus in nanofibrous mats while maintaining high porosity. © 2015 Wiley Periodicals, Inc. J. Polym. Sci., Part B: Polym. Phys. **2016**, *54*, 787–796

KEYWORDS: annealing; carbon nanotubes; crystallinity; mechanical properties; nanofibers

INTRODUCTION Electrospinning is a simple and versatile process suitable for many polymer materials that can produce ultra-fine fibers with a broad range of diameters.[1,2] Due to the nanofibrous morphology, electrospun nanofibrous membranes (or webs) possess unique properties, such as high relative surface area-to-volume ratio, and a three-dimensional highly porous structure.[3] Due to this unique structure, electrospun nanofibrous webs have been utilized in a variety of applications such as filtration, tissue engineering scaffolds, drug release, wound dressings, nano-sensors (including thermal sensors, strain sensors, chemical vapor sensors), military protective clothing, cosmetic skin masks, and other industrial applications.[1]

Electrospun nanofibrous mats sometimes lack the necessary mechanical properties for practical applications. Annealing is one method of post treatment frequently applied to electrospun webs to enhance their properties. The differences in annealing method can include time, temperature, the presence or absence of applied tension (constrained or unconstrained) during annealing, the medium to conduct heat to and away from the sample (water, air, or a specific fluid to maintain dimensional stability), or pairing with other post treatments (e.g., initial drawing).

A review of the literature indicates that very few researchers have studied the effect of applied tension to the web during annealing.[4,5] Constrained annealing has been performed for single fibers,[6,7] where the crystal structure inside the fiber is the unique factor affecting mechanical properties. Statton et al.[6] compared properties of highly drawn poly(ethylene terephthalate) (PET) fibers annealed at high temperatures while under three different degrees of tension; slack (free to shrink), taut (held at constant length) and tensioned (to achieve a 10% increase in length while at the elevated temperature). Babatope et al.[7] compared tensile modulus of nylon6-6 fibers annealed at increasing temperatures while constrained (taut) and unconstrained (slack). For electrospun webs, mechanical properties can be affected by crystal structure, molecular alignment of the amorphous chains, fiber alignment, and inter-fiber bonding. Often as-spun webs (without any treatment) display molecular alignment along the fiber axis. Zong et al.[5] compared mechanical properties between as-spun webs and those drawn and annealed (tensioned) with a focus on fiber

alignment and molecular orientation. Ramaswamy et al.[4] compared mechanical properties between as-spun webs and those annealed without constraint (slack) with a focus on inter-fiber bonding and molecular orientation.

Nanocomposites, with the aim of improving the properties of polymer matrices, have attracted tremendous attention for more than a decade. Nanofillers ranging from metal particles to organometallic clays and carbon materials have been investigated.[8,9] Multiwall carbon nanotubes (MWNTs) have been of interest due their unique combination of desirable properties (mechanical and electrical) and relative ease of dispersion (relative to single-wall carbon nanotubes).[4,10–12] In order to translate the properties of the carbon nanotube to macro-scale structures, one of the biggest challenges remains carbon nanotube (CNT) dispersion in the polymer matrix. Often the homogeneous dispersion of nanotubes is limited by both the synthesis induced "entangled" and "aggregated" structures of nanotubes as well as their tendency to form agglomerates, due to the intermolecular van der Waals interactions between tubes. Many researchers have studied various surfactants for CNT dispersion, such as Gum Arabic (GA) (a polysaccharide blend),[13] standard DNA (sDNA),[14] and sodium dodecyl sulfate (SDS).[15] As for mechanical methods, ultrasonication is a common technique for dispersing CNTs in solvents by both breaking up CNT aggregates and shortening tubes which will then be less likely to entangle and agglomerate. Kumar et al. recently utilized an ultrasonication bath in excess solvent (around 40 times larger than required) to obtain a homogeneous SWNT dispersion solution and then evaporated the excess solvent by vacuum distillation to obtain an almost ideal dispersion.[16] For faster (and likely, less efficient) schemes for dispersion, an alternative paradigm is to characterize the volume % of well-dispersed, un-entangled MWNT and the number and size of aggregates. In this manner, the mechanical enhancement due to the MWNT can be understood in this sub-optimal but more realistic condition. In this work, such an approach is taken: the common practice of sonicating with GA present is utilized and the resulting dispersion is characterized and connected to observed mechanical properties.

An extensive comparison between as-spun webs and webs annealed while unconstrained (slack) and constrained (taut) is presented here, for both neat fibers and those doped with various concentrations of MWNT. The MWNT effect is interpreted with the help of dispersion analysis. Decoupling the effect of fiber alignment (and molecular orientation) from that due to inter-fiber bonding and determining how these changes are altered by the presence of MWNT is the focus of this work. Importantly, under these annealing conditions, crystallinity is not enhanced (in contrast with single fiber studies) and fiber–fiber bonding, fiber alignment and existing molecular alignment within fibers lead to changes in mechanical properties.

EXPERIMENTAL

Mat Fabrication

Poly(ethylene oxide) (PEO) of M_w 400,000 g/mol was purchased from Scientific Polymer Products. MWNT with a diameter of 15 ± 5 nm, a length of 5–20 μm, and a density of 1.34–1.35 g/cc at 95% purity were obtained from NanoLab.[17] GA provided by Sigma Aldrich was used as dispersant. Deionized water was the only solvent used in solution preparation.

Electrospinning solutions were prepared in two equal parts (by mass) by mixing a MWNT/GA solution with a PEO solution. First, different concentrations of MWNTs were added to 3 wt % GA (relative to the total mass) solution. The MWNT/GA solution was sonicated for 30 min using an Ultrasonicator Model 2000U producing 175 watts [average power(RMS)] output power in water with a 5 T Standard Probe operating at 25 Hz. Concurrently, PEO was dissolved in deionized water. Then PEO solution was poured into the homogeneous GA/MWNTs suspensions and mixed by magnetic stirrer. The final solutions consisted of 6 wt % PEO (relative to the total mass of the solution) with concentrations of MWNTs ranging from 0 to 3 wt % relative to the polymer mass, and 1.5 wt % GA relative to the total mass.

The prepared solutions were loaded in 10 mL syringes fixed by luer-lock connections and pumped into a 4 inch 20 gauge blunt tip needle. The syringe pump was obtained from New Era Pump systems (model NE 500). The high-voltage power was supplied from Glassman (High Voltage Model FC60R2 with a positive polarity). The electrospinning parameters for MWNT/PEO solutions were as follows: applied voltage ranging from 12 to 14 kV; a working distance (the distance between the needle and the collector plate) of 19.5 cm; and a solution feed rate of 7 μL/min. Aluminum foil was placed over the grounded collector plate to collect the unoriented (random) electrospun mats. The electrospinning time was 5 hours to produce sufficiently thick webs ($\sim$250 μm) for mechanical measurements.

Annealing Treatment

A convection oven (LR Technologies, Model LN 60) was used to anneal the specimens. Samples were heated under the presence or absence of tension (constrained and unconstrained annealing). For unconstrained annealing, samples (1 cm $\times$ 6 cm, cut from the electrospun web) were loaded into a preheated petri dish layered with Teflon tape in a convection oven at the specified annealing temperature for 4 min. Teflon tape was used to prevent samples from sticking to the glass and thus the sample could shrink freely. After heat treatment, the annealed web was then mounted onto a paper frame for mechanical testing (Fig. 1). For calculation of the mechanical properties, the length, width, and thickness were measured after annealing and mat shrinkage. For constrained annealing, the samples (also 1 cm $\times$ 6 cm) were attached to the paper frame (Fig. 1) before thermal treatment to constrain the specimen length during annealing. Samples were subsequently placed in the preheated petri dish layered with Teflon tape in the convection oven at the specified annealing temperature for 4 min. Original sample dimensions were used to calculate the mechanical properties. To express each condition more simply, abbreviations are used. For example, "60unc" indicates "Unconstrained

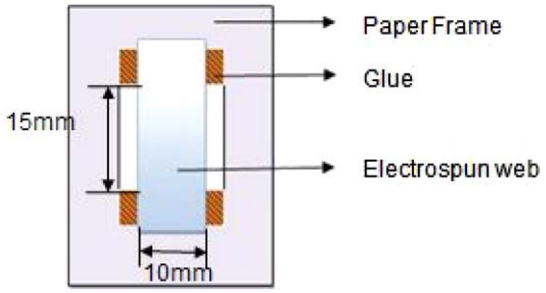

FIGURE 1 Schematic diagram of the paper frame used for annealing and mechanical testing. [Color figure can be viewed in the online issue, which is available at wileyonlinelibrary.com.]

Annealing at 60 °C" and "64con" indicates "Constrained Annealing at 64 °C."

Characterization

The fiber morphology, porosity, and fiber diameter of MWNT/PEO webs obtained from electrospinning were characterized using a scanning electron microscope (SEM, JEOL model JSM-6400 FE w/EDS) operating at 5 kV. The electrospun samples were sputter-coated with approximately 100 Å of Au/Pd to reduce charging. Images were analyzed using NIH Image J™ Software. Fiber diameter was the average value of 50 points randomly selected from at least two SEM images. The porosity of the electrospun webs was also measured by Image J™ as reported previously.[4,18]

Transmission electron microscopy (TEM) was performed using FEI/Philips EM 208S operating at 80 kV to observe MWNTs within the nanofiber as a function of MWNT concentration. The nanofiber sample was prepared by directly electrospinning on copper grids coated with lacey carbon. TEM images were processed using Image J™ to estimate the volume fraction of "free" (non-aggregated) MWNTs in the PEO nanofiber, MWNT aggregate cluster size, and the number of MWNTs aggregates per unit volume. For each specific concentration of MWNTs in the PEO nanofiber mat, images of eight nanofibers were used to estimate the volume fraction of free MWNTs. The number of non-aggregated (single) MWNTs in each nanofiber was determined and the estimated volume fraction of the free MWNTs for that nanofiber was calculated using the total volume of the free MWNTs divided by the total nanofiber volume. The final estimated vol % of free MWNTs was the average value from the eight, randomly selected nanofibers. An estimate of the MWNT aggregate cluster size was made by calculating the area of nanotube clusters (identified as dark bundles in the TEM images) from the measured length and width of the bounding rectangular area covering the selected aggregation region. The estimate reported is an average of at least eight MWNT clusters. The number of MWNTs aggregates per volume was calculated using the ratio of the number of aggregated MWNT clusters to the total volume of fibers from eight different TEM images.

The melting temperatures and degree of crystallinity of PEO in the original pellet form, as-prepared PEO webs, and post-treated electrospun PEO webs were measured using a Perkin Elmer Diamond Differential Scanning Calorimeter (DSC). The samples were heated from −20 °C to 80 °C at a heating rate of 20 °C/min. The melting temperature is identified by the endothermic peak in the DSC curve. The degree of crystallinity was calculated by dividing the heat of fusion of each sample by the heat fusion of perfectly crystalline PEO (205 J/g).[19]

An Omni ATPS, XRD 1000(Model\# PH268L-25) X-ray apparatus with a proportional counter was utilized for the wide angle X-ray Diffraction study using a Cu Kα X-Ray Anode with the wavelength (λ) of 1.54 Å. The scanning angle (°) ranged from 5° to 40° with 0.1° step size. From the WAXD intensity as a function of 2θ, the d-spacing [from the Bragg equation (eq 1)]; full-width at half the maximum intensity (FWHM), β; Peak I (∼19.5°)/Peak II (∼23.5°) intensity ratio; and average crystallite size (ACS) [from the Scherrer equation (eq 2)] were reported. Peak I/Peak II intensity ratio is the ratio of the intensity for the peak at roughly 19.5° (Peak I) and 23.5° (Peak II).

The Bragg equation is as follows:

$$d = n\lambda/(2\sin\theta) \tag{1}$$

where n is the integral diffraction order (equal to 1), λ is the X-ray wavelength, and θ is the scanning angle.

The Scherrer equation is as follows:

$$\mathrm{ACS} = K\lambda/\beta\cos\theta \tag{2}$$

where K is the shape factor, 0.9 here, and β is the full-width at half the maximum intensity.

Modulus and maximum tensile strength of treated webs were measured with universal tensile testing machine (Instron Model 5544 using the Bluehill version 2.0 software). Rectangular samples were prepared with a gauge length of 1.5 cm, a sample width of 1.0 cm, and a thickness ranging from 0.1 to 0.3 mm. A caliper was used to measure the length and width of samples with the precision of 0.1 mm and the thickness was measured with a thickness gauge (Mitutoyo absolute Digimatic thickness gauge, No.543-394B, with the accuracy of 0.003 mm and measuring force of 0.7 N). For each sample, five specimens were tested at a constant displacement rate of 10 mm/min, within 24 hours of fabrication. Due to the variance of thicknesses within one mat and different mats, the thickness of each individual electrospun specimen was measured before mechanical testing with the thickness gauge. The cross-sectional area was calculated as follows: $A = t \times w \times (1 - P)$ where: t is the thickness of the sample; w is the width of the sample; and P is the porosity of electrospun web (ranging from 0 to 1).

RESULTS AND DISCUSSION

Fiber and Web Characterization

Table 1 summarizes fiber diameters of electrospun webs manufactured with the incorporation of 0–3 wt % MWNTs.

TABLE 1 Fiber Diameters for as Spun PEO and MWNT/PEO Nanofibers

MWNTs (wt %)	Fiber Diameter (nm)
0	213 ± 24
0.25	190 ± 29
0.5	260 ± 26
1.0	225 ± 51
1.5	229 ± 43
2.0	193 ± 32
3.0	191 ± 30

The SEM images in Figure 2 show that the electrospun mats retain nanofibrous structure with the addition of MWNT loadings up to 3 wt %. The addition of MWNTs increases the solution conductivity which results in a gradual (although non-significant) decrease in fiber diameter, as expected.[20]

Qualification of Free and Aggregated MWNTs in the Electrospun Fibers

Figure 3(a–c) summarizes TEM images of MWNT/PEO electrospun with 0.25%, 1.5%, and 3% MWNTs respectively. It is evident that the MWNTs were successfully embedded in the electrospun nanofiber from the GA/PEO solution and are relatively oriented along the fiber axis but with some degree of entanglement. (In Fig. 3, arrows indicate location of MWNTs.) Such MWNT conformations in electrospun nanofibers were also observed by Dror et al. and Sung et al.[15,21] In Figure 3(a–c), the increase in the MWNT density with an increase in the concentration of MWNTs in the GA/PEO solution can be visually observed. The number of individual (unentangled) MWNTs (referred to as the free MWNT vol %), the average MWNT aggregate size, and the number of aggregates per unit volume were estimated by TEM image analysis and are summarized in Table 2. The estimated volume fractions of free MWNTs from TEM images are lower than the calculated concentration due to the fact that a significant fraction of the MWNTs are aggregated (and hence are not considered "free MWNTs") in addition to the error associated with physically counting the nanotubes. The estimates in Table 2 indicate that the average aggregate size is independent of MWNT loading (1.5 and 3.0 wt % MWNT), however the number of aggregates per unit volume increases with increasing MWNT concentration. Further, as is shown by the estimate of free MWNTs, an increase in MWNT concentration does not necessarily increase the number of free nanotubes proportionally.

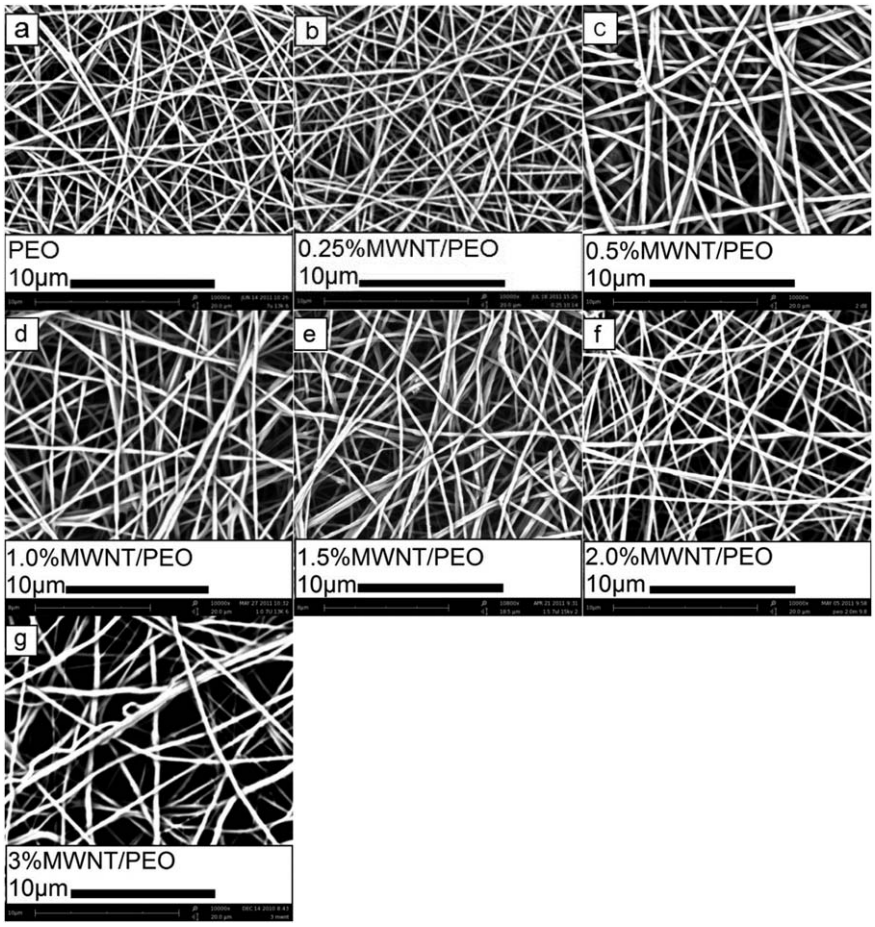

FIGURE 2 Morphology of PEO as-spun fiber webs with different concentrations (wt %) of MWNT: (**a**) 0, (**b**) 0.25, (**c**) 0.5, (**d**) 1.0, (**e**) 1.5, (**f**) 2.0, and (**g**) 3.0.

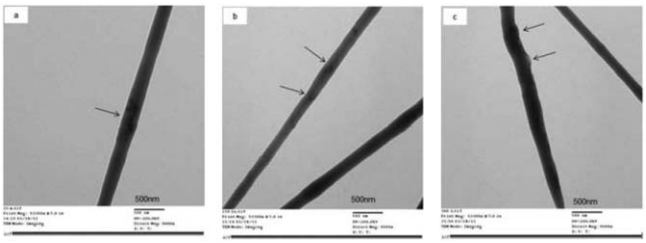

FIGURE 3 TEM Images of the MWNTs/PEO composite nanofibers with (**a**) 0.25 wt %, (**b**) 1.5 wt %, and (**c**) 3.0 wt % MWNTs in the nanofibers, respectively. The scale bar is 500 nm.

Thermal Properties of Electrospun Webs

PEO is semi-crystalline polymer, and to introduce the inter-fiber bonding (at relatively short times), an annealing temperature must be set near the melting temperature (T_m).[22,23] Differential scanning calorimetry was performed to determine the T_m of electrospun MWNT/PEO webs. As shown in Figure 4 and Table 3, the largest effect on T_m is the addition of GA (used as a surfactant to disperse the MWNT). The addition of only 1.5 wt % GA (relative to total mass) significantly decreases the melt temperature (from 72 °C to 62 °C) as well as the overall crystallinity (from 70% to 58%) of electrospun mats. This is attributed to GA's highly branched structure which disrupts PEO's ability to crystallize. The fact that this happens at such low concentrations is of note. In contrast, the melting temperature of electrospun PEO webs (62 °C ± 1 °C) only increases slightly (~2 °C) with increasing MWNT concentration (up to 3 wt %). When comparing electrospun membranes with the as-received PEO (in pellet form), it is observed that the Tm of neat electrospun mats (72 °C) is similar to that of the PEO pellet (71 °C) and the crystallinity of nanofibrous mats (70%) is lower than that of the PEO pellet (89%). The lower crystallinity in electrospun webs indicates the suppression of forming crystal structure during the electrospinning process, which agrees with previous results.[4,24,25]

Constrained Versus Unconstrained Annealing

Melt Temperature and Crystallinity Fraction

Annealing treatments on electrospun PEO webs were performed from 60 °C to 64 °C (for 4 minutes). There is no significant trend in T_m or the crystallinity of PEO webs subjected to constrained or unconstrained annealing as a function of annealing temperature (Table 4). In fact, crystallinity trends downward for the unconstrained samples and upward for the constrained samples, which could be attributed to strain-induced crystallization. In addition, when 0.25 wt% MWNTs are added, similar results to those seen in PEO/GA-only webs are observed, that is, no significant change in either T_m or crystallinity fraction (Table 5).

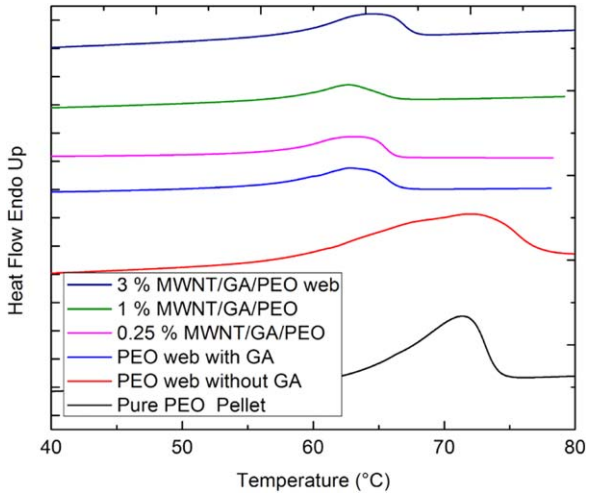

FIGURE 4 DSC thermograms of as received PEO (pellet), PEO web without GA and 0%–3% MWNT/PEO web with GA. The legend lists the data shown in order from top to bottom. [Color figure can be viewed in the online issue, which is available at wileyonlinelibrary.com.]

Mat Morphology and Fiber Alignment

Figure 5 shows SEM images of membranes electrospun from 6% PEO/1.5% GA solutions and thermally treated for the different annealing conditions. The progression of thermal bonding can be viewed as temperature increases. Between 60 °C and 62 °C, nanofibers start relaxing and surface bonding at fiber junctions begins to occur. At 63 °C, significant fiber–fiber bonding is evident, where the number of fiber–fiber bonding points increase, relative to that at 62 °C. At 64 °C, cohesive bonding from overlapping fibers (fiber–fiber fusion) occurs at most nanofiber intersections. Upon increased annealing temperature, the number of fiber–fiber bonds across the web increases and the mats shrink, a process which is driven by thermally induced molecular relaxations of the polymer chains, which are elongated and aligned

TABLE 2 Estimated Volume Fraction of the Free MWNTs, Size of MWNT Aggregates, and the Number of Aggregates Per Unit Volume in the PEO Nanofibers Based on TEM Images ($N = 8$)

MWNTs (wt %)	Calculated MWNT (vol %)	Estimated Free Non-Aggregated MWNT by TEM (vol %)	Aggregate Length (nm)	Aggregate Width (nm)	Number of Aggregates Per Volume (nm^{-3})
0.25	0.23	0.14 ± 0.11	370 ± 60	210 ± 45	2.80E-09
1.5	1.38	1.16 ± 0.07	330 ± 45	270 ± 45	3.62E-09
3.0	2.79	0.60 ± 0.18	440 ± 65	270 ± 40	5.10E-09

TABLE 3 T_m (±1 °C) and % Crystallinity (±2%) Obtained From DSC Thermograms of PEO Pellet, PEO Web Without GA and 0%–3.0% MWNT/PEO Web with GA

Material	T_m (°C)	Crystallinity (%)
PEO (pellet)	71	89
PEO web	72	70
PEO/GA web	62	58
0.25% MWNT/PEO/GA web	63	60
1.0% MWNT/PEO/GA web	63	57
3.0% MWNT/PEO/GA web	64	52

TABLE 4 T_m (±1 °C) and % Crystallinity (±2%) Obtained From DSC Thermograms of Electrospun PEO Mats Subjected to Unconstrained or Constrained Annealing as a Function of Temperature

	Unconstrained Annealing		Constrained Annealing	
Annealing Temperature (°C)	T_m (°C)	Crystallinity (%)	T_m (°C)	Crystallinity (%)
60	64	67	63	60
62	65	67	64	62
63	65	65	65	65
64	65	62	65	66

along the fiber axes in the as-spun web.[5,26,27] Compared with unconstrained annealing, which allows the webs to shrink freely (due to molecular relaxations) during heat treatment, constrained annealing applies a tension to the web which induces nanofiber orientation along the constraint direction [Fig. 5(e–h)] as the web attempts to shrink during annealing. Importantly, although this partial alignment of the fibers results in significant changes in mechanical properties

TABLE 5 T_m and % Crystallinity Obtained From DSC Thermograms of Electrospun 0.25% MWNT/PEO Mats Subjected to Unconstrained or Constrained Annealing as a Function of Temperature

	Unconstrained Annealing		Constrained Annealing	
Annealing Temperature (°C)	T_m (°C)	Crystallinity (%)	T_m (°C)	Crystallinity (%)
60	65	64	64	62
62	65	62	65	61
63	66	65	66	62
64	66	60	66	61

(section "Strength and Modulus"), particularly enhanced modulus, for optimal conditions (63 °C) the porosity of the web is maintained (Table 6). Thus one effect of the presence of constraint is maintenance of high porosity over a relatively large annealing temperature range. In Figure 5, all images were chosen from the center of the web. When scanning the whole web (not shown here), it was seen that at 60 °C and 62 °C, a high degree of nanofiber alignment only occurred at the top and bottom edges of the constrained samples, but at 64 °C, the partial fiber alignment gradually spread across the whole web, as depicted in Figure 5(h).

Porosities of as-spun and post-treated PEO electrospun membranes are summarized in Table 6. There is no significant change in web porosity until the annealing temperature reaches 64 °C, at which point the porosity decreases, which is consistent with the observation of partial nanofibers fusion at some points in the SEM images (Figure 5, 64con). Constrained samples maintain porosity better than unconstrained samples. The change in web morphology and porosity after annealing for 0.25% MWNT/PEO and 1.0% MWNT/

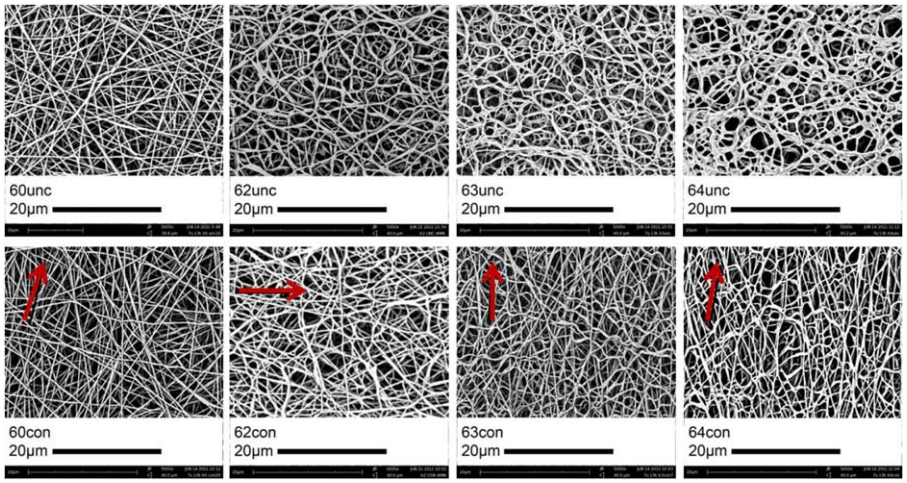

FIGURE 5 SEM images of electrospun PEO nanofibers as a function of unconstrained annealing at (**a**) 60 °C, (**b**) 62 °C, (**c**) 63 °C, and (**d**) 64 °C and constrained annealing at (**e**) 60 °C, (**f**) 62 °C, (**g**) 63 °C, and (**h**) 64 °C. All images were taken at the center of the electrospun webs. The *arrow* indicates the constraint axis during annealing (for constrained samples). [Color figure can be viewed in the online issue, which is available at wileyonlinelibrary.com.]

TABLE 6 Comparison of Overall Porosity (%) for Post-Treated PEO Electrospun Mats; the Post-Treatments Involved Unconstrained Annealing and Constrained Annealing at Different Temperatures

	Porosity	
Annealing Temperature (°C)	Unconstrained	Constrained
60	74 ± 1.6	76 ± 1.1
62	72 ± 2.3	77 ± 1.6
63	74 ± 2.0	77 ± 0.6
64	67 ± 2.0	61 ± 1.7

PEO webs is consistent with the results observed on neat PEO webs (images are not included in this article).

Structure of the Matrix

The structure and orientation of crystallinity are studied using wide angle X-ray diffraction. Figure 6 depicts the WAXD profiles of electrospun PEO webs before and after constrained or unconstrained annealing at 63 °C and 64 °C. The WAXD pattern of the as-spun PEO web has a peak at approximately 19° (referred to as Peak I) and a peak at approximately 23° (referred to as Peak II). According to previous work[28,29] and verified by calculation, the peak near 19° is from the (120) reflections and the peak near 23° is a combination of the PEO (112) and (032) reflections (Fig. 6). There is no significant change in WAXD patterns of post-treated PEO webs, except the varying intensity ratio of Peak I/II under different annealing conditions (as shown in Table 7).

Nanofibrous PEO webs subjected to constrained annealing at 63 °C possess the highest peak I/II ratio (15.36) (from Table 7). Acierno et al. attributed the change in the intensity ratio of different planes to a slight orientation of the crystals along the fibers.[30] Thus, this observation is consistent with the constrained samples having a higher degree of fiber orientation as shown in the SEM studies (Fig. 5). Because of existing molecular orientation within the fibers due to the

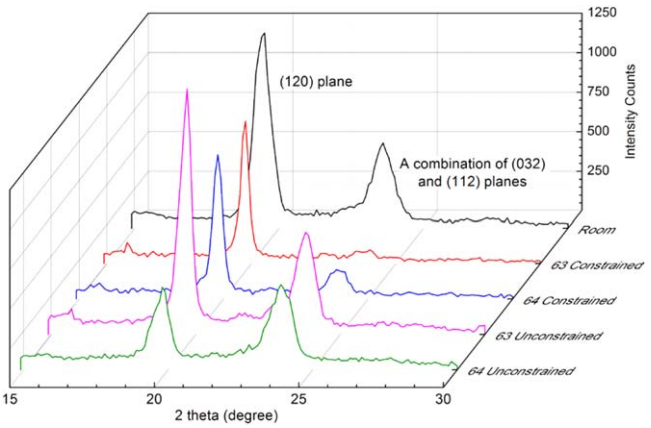

FIGURE 6 WAXD profiles of electrospun PEO webs unannealed (room) and annealed (both constrained and unconstrained) at 63 °C and 64 °C. [Color figure can be viewed in the online issue, which is available at wileyonlinelibrary.com.]

electrospinning process, crystallites will also have some alignment along the fiber axis. Fiber alignment then orients both the extended amorphous material and crystallites within each fiber along a macroscopic sample direction (the direction of the tension imposed due to the constraint). In contrast, unconstrained annealing at 63 °C resulted in no change in the Peak I/II ratio from the as-spun sample. These effects are also seen for samples annealed at 64 °C where the Peak I/II ratio due to confined annealing is more than two times that for the un-annealed samples. Unconstrained annealing at 64 °C resulted in a Peak I/II ratio (0.97), similar to that for the PEO powder (~0.9) with the randomly oriented crystallites as reported previously,[31] and lower than the as-spun webs. This is consistent with no fiber alignment, and in fact, thermally-induced relaxation of the elongated chains (present in the as-spun samples) within each fiber during unconstrained annealing. Thus constrained annealing at 63 °C results in the optimal effect, sufficient heating to allow fiber alignment under the applied tension of confinement, but not enough thermal energy to allow relaxation of the existing elongated chains.

TABLE 7 Peak angle (2θ), d-Spacing, FWHM, and ACS for Peak I and II, and Peak I/II Ratio, From WAXD Patterns of As-Spun and Annealed (Constrained or Unconstrained) PEO Mats at 63 °C and 64 °C

Sample	Peak	2θ (°)	d-Spacing (Å)	FWHM (°)	ACS (Å)	Peak I/Peak II Ratio
As-spun PEO	I	19.4	4.57	0.64	124.5	2.28
	II	23.6	3.78	0.83	96.6	
PEO 63 °C: unconstrained	I	19.6	4.52	0.46	173.2	2.39
	II	23.7	3.74	0.79	101.6	
PEO 64 °C: unconstrained	I	19.8	4.48	0.70	113.9	0.97
	II	23.8	3.73	0.87	92.2	
PEO 63 °C: constrained	I	19.8	4.48	0.32	249.1	15.36
	II	23.9	3.72	1.10	80.3	
PEO 64 °C: constrained	I	19.8	4.49	0.37	215.4	4.81
	II	23.9	3.72	0.65	123.5	

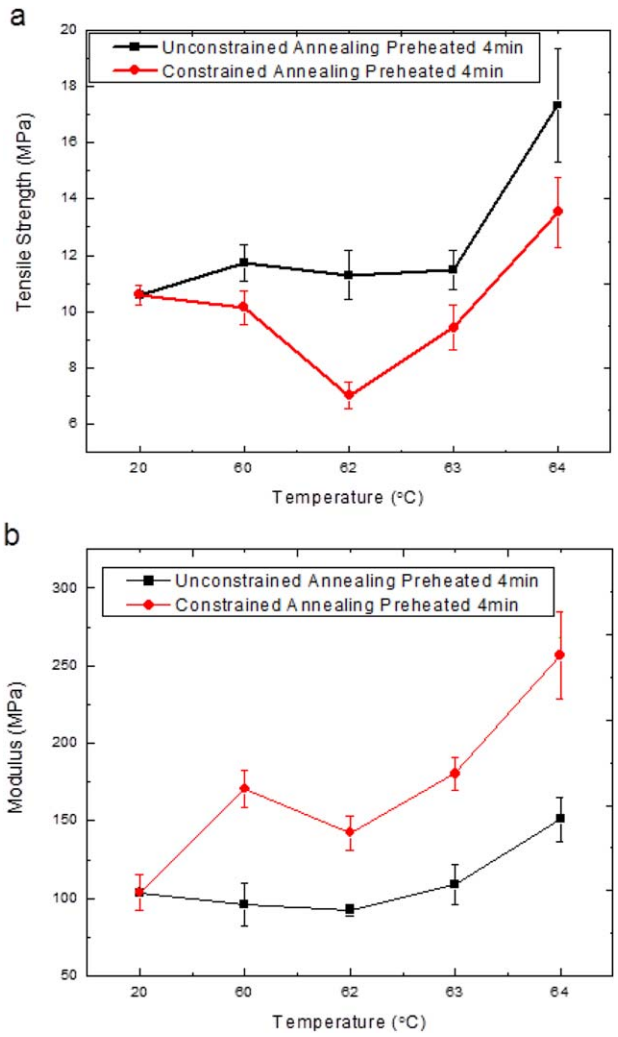

FIGURE 7 Tensile strength (**a**) and modulus (**b**) of electrospun PEO mats as a function of annealing temperature for different annealing treatments. The error bars represent standard error. [Color figure can be viewed in the online issue, which is available at wileyonlinelibrary.com.]

PEO webs with MWNTs do not show a significant increase in Peak I/II ratio (compared with unannealed samples with same MWNT content) upon constrained annealing at 63 °C. A potential explanation for this may be that MWNTs anchor the crystalline domains in the nanofibers and more strongly restrict the reorientation of crystalline domains upon constrained annealing.

Tables 7 and 8 also show more subtle changes in Bragg angle, the peak broadness as determined from the FWHM, and the resulting average crystallite size (ACS). As expected, annealing improves the packing and increases the size of the PEO crystalline domains, as evidenced by the shifting of the Bragg angle to higher angles, a decrease in d-spacing, an increase in ACS, and a sharper peak around 19°, in almost all cases with and without the presence of MWNT. Relaxation due to heating at the melting point, as discussed above, may be reflected in the differing trends for unconstrained annealing at 64 °C. For the lowest concentration (0.25 wt%) of MWNT, constrained annealing at 63 °C results in the same trends observed for neat PEO. For higher loading (1 wt%) the results are more complex, indicating that the presence of MWNT at a significant level alters the details of the crystallization and annealing processes.

Strength and Modulus

Figure 7 shows the tensile strength and modulus of electrospun PEO mats as a function of annealing temperature for both unconstrained and constrained annealing. All samples show no significant change in tensile strength until 64 °C. The increase in strength at 64 °C is attributed to apparent fiber–fiber fusing (as seen in Fig. 5), decreasing mat delamination under tension, and the resulting drop in mat porosity (Table 6). Figure 8 compares these mechanical properties with electrospun mats containing MWNTs. From the data, it is clear that the addition of MWNTs to PEO had no significant effect on the tensile strength for both as spun and annealed samples. As is the case for PEO mats, the tensile strength of MWNT/PEO mats also significantly increases only at 64 °C, which is consistent with fiber–fiber fusing of the nanofibers in the mat.

The PEO mat modulus [Fig. 7(b)] generally increases with annealing temperature for the constrained samples while there is no significant change for unconstrained annealing until 64 °C. The linear increase in modulus as temperature increases (also described below for MWNT-containing

TABLE 8 Peak Angle (2θ), d-Spacing, FWHM, and ACS for Peak I and II, and Peak I/II Ratio, From WAXD Patterns of As-Spun and Annealed (Constrained Only) PEO Mats (with 0.25 and 1.0% MWNTs) at 63 °C

Sample	Peak	2θ (°)	d-Spacing (Å)	FWHM (°)	ACS (Å)	Peak I/Peak II Ratio
0.25% MWNT/PEO	I	19.6	4.52	0.65	122.9	2.20
	II	23.6	3.76	1.06	75.7	
0.25% MWNT/PEO 63 °C: constrained	I	19.7	4.50	0.43	185.0	2.06
	II	23.9	3.72	0.94	85.4	
1% MWNT/PEO	I	20.0	4.44	0.44	179.5	3.45
	II	24.1	3.69	0.74	108.5	
1% MWNT/PEO 63 °C: constrained	I	19.8	4.48	0.46	173.8	4.08
	II	23.8	3.73	0.87	92.2	

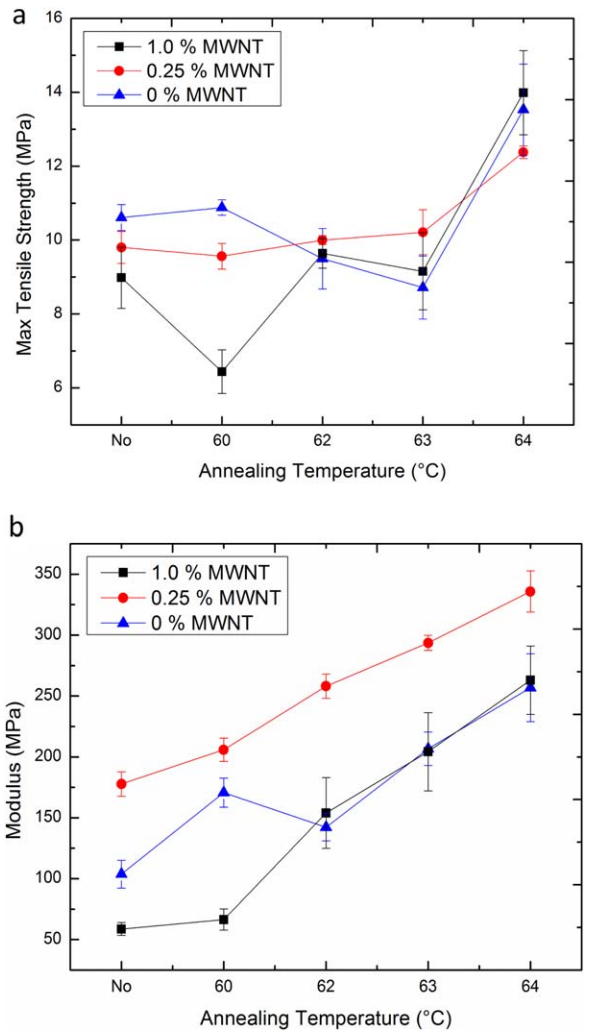

FIGURE 8 Tensile strength (**a**) and modulus (**b**) of electrospun PEO, 0.25% and 1% MWNT/PEO mats as a function of constrained annealing temperature. The error bars represent standard error. [Color figure can be viewed in the online issue, which is available at wileyonlinelibrary.com.]

samples) in the constrained case is attributed to fiber alignment under tension, which also orients the aligned molecules within the electrospun fibers along the tension direction, as supported by the WAXD and SEM studies discussed above. Even at 64 °C, where the unconstrained samples exhibit an increased modulus (presumably associated with fiber–fiber bonding, Fig. 5), constrained annealing results in a 150% increase in modulus compared with a 46% increase for the unconstrained samples. At lower temperatures (below 63 °C), the irregular response may result from alignment being present only at the sample edges as discussed in the context of Figure 5.

Addition of 0.25 wt% MWNT increases the modulus under all conditions [Fig. 8(b)] while the 1.0% MWNT:PEO webs have a similar modulus to that of neat PEO. This is attributed to better dispersion of MWNTs at lower concentrations as reported earlier[13] and qualitatively estimated here. At 0.25 wt% the MWNT are isolated and tend to be aligned along each fiber axis (Fig. 3). Constrained annealing improves the modulus of PEO mats with 0.25 wt % and 1.0 wt % MWNTs [Fig. 8(b)], in a similar manner as shown for the neat PEO mats. Again, constrained annealing orients the fibers to the tension axis, placing the existing aligned molecules and MWNT along the tension direction. The alignment of both MWNT and molecular chains along the tension direction leads to a strongly enhanced modulus. Overall, the fiber alignment along the tension direction and the existing molecular orientation effectively improve the modulus of the nanofibrous mats (both with and without MWNTs) but do not significantly alter strength. In contrast, strong fiber–fiber fusion (the dominant effect due to unconstrained annealing) contributes more directly to strength development.

CONCLUSION

Electrospun mats with and without MWNT often have poor mechanical properties. Annealing is a simple strategy to improve strength and modulus. Increases in nanofibrous mat strength were obtained from fiber–fiber bonding due to annealing near the melting point (with the associated loss of some fibrous morphology). More interestingly, annealing near T_m under a minor constraint (the presence of paper frame) leads to fiber alignment which resulted in significant increases in modulus as the fibers, the aligned molecules within them, and well-dispersed MWNT if present became oriented along the tension axis. In particular, constrained annealing at temperatures just below the melting point resulted in fiber alignment due to the imposed tension when the mat was unable to spontaneously shrink. Because of the apparent sensitivity of such systems to even minor constraint (such as unintentional adhesion to a dish in which annealing is performed), these results indicate that in order to fully interpret annealing results, the effect of possible inadvertent tension applied during annealing should be considered. In fact, constrained annealing may be a strategy to facilely enhance modulus while still retaining much of the innate random nanofibrous morphology, such as high porosity and high specific surface area.

ACKNOWLEDGMENTS

The authors acknowledge the use of the Analytical Instrumentation Facility (AIF) at North Carolina State University, which is supported by the State of North Carolina and the National Science Foundation. The authors also acknowledge Ms. Birgit Andersen for assistance with differential scanning calorimetry.

REFERENCES AND NOTES

1 J. He, Y. Liu, L. Xu, *Mater. Sci. Technol.* **2010**, *26*, 1275–1287.

2 C. J. Luo, S. D. Stoyanov, E. Stride, E. Pelan, M. Edirisinghe, *Chem. Soc. Rev.* **2012**, *41*, 4708–4735.

3 Z. M. Huang, Y. Z. Zhang, M. Kotaki, S. Ramakrishna, *Compos. Sci. Technol.* **2003**, *63*, 2223–2253.

4 S. Ramaswamy, L. I. Clarke, R. E. Gorga, *Polymer* **2011**, *52*, 3183–3189.

5 X. Zong, S. Ran, D. Fang, B. Hsiao, B. Chu, *Polymer* **2003**, *44*, 4959–4967.

6 W. Statton, *J. Polym. Sci. Part C-Polym. Symp.* **1971**, *32*, 219.

7 B. Babatope, D. Isaac, *Polymer* **1992**, *33*, 1664–1668.

8 F. Hussain, M. Hojjati, M. Okamoto, R. E. Gorga, *J. Compos. Mater.* **2006**, *40*, 1511–1575.

9 M. Moniruzzaman, K. I. Winey, *Macromolecules* **2006**, *39*, 5194–5205.

10 S. D. McCullen, D. R. Stevens, W. A. Roberts, L. I. Clarke, S. H. Bernacki, R. E. Gorga, E. G. Loboa, *Int. J. Nanomed.* **2007**, *2*, 253–263.

11 S. D. McCullen, K. L. Stano, D. R. Stevens, W. A. Roberts, N. A. Monteiro-Riviere, L. I. Clarke, R. E. Gorga, *J. Appl. Polym. Sci.* **2007**, *105*, 1668–1678.

12 S. S. Ojha, D. R. Stevens, K. Stano, T. Hoffman, L. I. Clarke, R. E. Gorga, *Macromolecules* **2008**, *41*, 2509–2513.

13 S. D. McCullen, D. R. Stevens, W. A. Roberts, S. S. Ojha, L. I. Clarke, R. E. Gorga, *Macromolecules* **2007**, *40*, 997–1003.

14 M. Zheng, A. Jagota, E. Semke, B. Diner, R. Mclean, S. Lustig, R. Richardson, N. Tassi, *Nat. Mater.* **2003**, *2*, 338–342.

15 Y. Dror, W. Salalha, R. Khalfin, Y. Cohen, A. Yarin, E. Zussman, *Langmuir* **2003**, *19*, 7012–7020.

16 H. Chae, M. Minus, S. Kumar, *Polymer* **2006**, *47*, 3494–3504.

17 Z. Huang, J. Wu, Z. Ren, J. Wang, M. Siegal, P. Provencio, *Appl. Phys. Lett.* **1998**, *73*, 3845–3847.

18 K. Yoon, K. Kim, X. Wang, D. Fang, B. Hsiao, B. Chu, *Polymer* **2006**, *47*, 2434–2441.

19 G. Vidotto, D. Levy, A. Kovacs, *Kolloid-Z. Z. Polym.* **1969**, *230*, 289

20 M. V. Jose, B. W. Steinert, V. Thomas, D. R. Dean, M. A. Abdalla, G. Price, G. M. Janowski, *Polymer* **2007**, *48*, 1096–1104.

21 J. H. Sung, H. S. Kim, H. Jin, H. J. Choi, I. Chin, *Macromolecules* **2004**, *37*, 9899–9902.

22 Y. You, S. Won Lee, S. Jin Lee, W. H. Park, *Mater. Lett.* **2006**, *60*, 1331–1333.

23 A. G. Mikos, Y. Bao, L. G. Cima, D. E. Ingber, J. P. Vacanti, R. Langer, *J. Biomed. Mater. Res.* **1993**, *27*, 183–189.

24 X. Zong, K. Kim, D. Fang, S. Ran, B. S. Hsiao, B. Chu, *Polymer* **2002**, *43*, 4403–4412.

25 N. Bhattarai, D. I. Cha, S. R. Bhattarai, M. S. Khil, H. Y. Kim, *J. Polym. Sci. Part B: Polym. Phys.* **2003**, *41*, 1955–1964.

26 P. F. Dismore, W. O. Statton, *J. Polym. Sci. Part B: Polym. Lett.* **1964**, *2*, 1113–1116.

27 S. Leporatti, C. Gao, A. Voigt, E. Donath, H. Möhwald, *Eur. Phys. J. E: Soft Matter Biol. Phys.* **2001**, *5*, 13–20.

28 E. Bortel, S. Hodorowicz, R. Lamot, *Makromol. Chem.* **1979**, *180*, 2491–2498.

29 M. V. Kakade, S. Givens, K. Gardner, K. H. Lee, D. B. Chase, J. F. Rabolt, *J. Am. Chem. Soc.* **2007**, *129*, 2777–2782.

30 D. Acierno, M. Lavorgna, F. Piscitelli, P. Russo, P. Spena, *Adv. Polym. Technol.* **2011**, *30*, 41–50.

31 J. Zhang, D. Yang, F. Xu, Z. Zhang, R. Yin, J. Nie, *Macromolecules* **2009**, *42*, 5278–5284.